Research Article

Mathematical Methods in the Applied Sciences

Received 27 March 2012

Published online 15 October 2012 in Wiley Online Library

(wileyonlinelibrary.com) DOI: 10.1002/mma.2697
MOS subject classification: 35J25; 78A70

Generalized eigenvalue decomposition of the field autocorrelation in correlation diffusion of photons in turbid media

N. Hyvönen[a*†], A. K. Nandakumaran[b], H. M. Varma[c] and R. M. Vasu[d]

Communicated by A. Kunoth

We propose a novel numerical method based on a generalized eigenvalue decomposition for solving the diffusion equation governing the correlation diffusion of photons in turbid media. Medical imaging modalities such as diffuse correlation tomography and ultrasound-modulated optical tomography have the (elliptic) diffusion equation parameterized by a time variable as the forward model. Hitherto, for the computation of the correlation function, the diffusion equation is solved repeatedly over the time parameter. We show that the use of a certain time-independent generalized eigenfunction basis results in the decoupling of the spatial and time dependence of the correlation function, thus allowing greater computational efficiency in arriving at the forward solution. Besides presenting the mathematical analysis of the generalized eigenvalue problem on the basis of spectral theory, we put forth the numerical results that compare the proposed numerical method with the standard technique for solving the diffusion equation. Copyright © 2012 John Wiley & Sons, Ltd.

Keywords: generalized eigenvalue decomposition; correlation diffusion of photons; correlation diffusion equation; ultrasound modulated optical tomography; diffuse correlation tomography

1. Introduction

Ultrasound-modulated optical tomography (UMOT) [1, 2] has been introduced to address the issue of poor spatial resolution in *diffuse optical tomography* (DOT) [3] images. In UMOT, one introduces a localized perturbation, with the help of a focussed *ultrasound* (US) beam, in the location of scattering centers and the refractive index (n), ultimately leading to a localized absorption coefficient (μ_a) and elasticity (Young's modulus E) measurement [4]. Even though UMOT looks like a straightforward extension of DOT for localized parameter recovery, it has a fundamental difference: whereas in DOT the basic dependent variable, the property of light, is the light fluence (I), in UMOT it is the field autocorrelation of light $\phi(x,\tau)$. Therefore, one can as well regard UMOT as an extension of *diffusing wave spectroscopy* (DWS) [5], wherein one studies dynamics in a turbid medium through following the decorrelation of $\phi(x,\tau)$ effected by dynamics in the object. In DWS, the dynamics is temperature-induced Brownian motion and the measurement is the intensity autocorrelation ($g_2(\tau)$) and the decay in $\phi(x,\tau)$ derived from $g_2(\tau)$ [6]. One can presently visualize UMOT as a system doing DWS with a localized deterministic perturbation brought in by the focused US beam.

The ultimate aim in UMOT is quantitative recovery of parameters (μ_a, E, etc.) pertaining to the focal region, the *region-of-interest* (ROI) of the US beam [7]. Toward this, a number of researchers have contributed, by way of deriving expressions for the modulation in n (Δn) and the displacement of scattering centers (**u**) in terms of the US forcing and the material properties [4, 8, 9], and also arriving at the *correlation transport equation* and its approximation, the *correlation diffusion equation* (CDE), which $\phi(x,\tau)$ obeys [10]. Both correlation transport equation and CDE have, like their counterparts in DOT, the *radiative transport equation* and its approximation the *diffusion equation* (DE) [3], the material property distributions appearing as coefficients. Therefore, these models open up the possibility of solving an inverse boundary value problem using UMOT data, that is, recovering μ_a and E distributions in the ROI from the boundary measurements of $g_2(\tau)$. (The US forcing in fact introduces a modulation in $g_2(\tau)$, and the modulation depth (M) in $g_2(\tau)$ is one of the possible UMOT measurements.)

[a] *Department of Mathematics and Systems Analysis, Aalto University, P.O. Box 11100, FI-00076 Aalto, Finland*
[b] *Department of Mathematics, Indian Institute of Science, Bangalore 560012, India*
[c] *ICFO – Institut de Ciències Fotòniques, Av. Carl Friedrich Gauss 3, 08860 Castelldefels, Spain*
[d] *Department of Instrumentation and Applied Physics, Indian Institute of Science, Bangalore 560012, India*
**Correspondence to: N. Hyvönen, Department of Mathematics and Systems Analysis, Aalto University, P.O. Box 11100, FI-00076 Aalto, Finland.*
[†] *E-mail: nuutti.hyvonen@aalto.fi*

We have recently attempted such tomographic recovery of the mean-square displacement distribution ($p(x)$) in the ROI (the displacement recovery is the first step toward the recovery of E) from the boundary measurement of M [11]. We have in fact very conveniently used the US perturbation to rewrite the CDE as a perturbation equation, connecting the perturbation in displacements to the perturbation in $\phi(x,\tau)$. The perturbation equation is solved iteratively to recover $p(x)$ in the ROI, with a spatial resolution limited to l^*, the transport mean free-path, owing to the use of CDE .

Unlike the DE of DOT, the CDE in UMOT has a temporal parameter, τ, the decorrelation time. Therefore, to construct $\phi(x,\tau)$, the CDE has to be solved for a range of values for τ. This is seen to be a heavy computational burden, making the iterative inversion almost prohibitively expensive, for it requires repeated forward solution of the CDE. This work is an attempt to reduce this computational overhead. Toward this, we reformulate the forward CDE problem as a (generalized) *eigenvalue problem* (EVP) and express $\phi(x,\tau)$ in terms of the corresponding eigenvalues and eigenvectors. The advantage gained is that the elliptic *partial differential equation* (PDE) defining the EVP is independent of τ. However, this new PDE also has to be solved for each of the eigenvectors, but fortunately, the number of eigenvectors needed to obtain a faithful representation of $\phi(x,\tau)$ is relatively low compared with the number of forward problems needed for handling the τ-dependence straightforwardly. This work puts forth a weighted eigenvalue formulation of the CDE resulting in a separation of τ from the spatial variables.

The main aim of this article is to carry out mathematical analysis of a generalized eigenvalue decomposition for a parameter-dependent second-order elliptic PDE. With UMOT as a possible application, the PDE considered here is the CDE in a turbid medium. However, this analysis is applicable in any context where the propagation model involves a temporal parameter (without a time derivative term), and the solution requires solving the PDE for an array of sample values for this parameter. We represent the solution of the CDE as an infinite series by using the eigenvectors corresponding to an elliptic PDE derived from the CDE. The crucial point to be considered here is that the eigenpairs are defined independently of the decorrelation time. This gives an enormous computational advantage in applications such as the DWS and UMOT image reconstructions, by reducing the overall time required to solve the forward problem. In this article, we present some computational results for the forward problem, demonstrating the anticipated advantage compared with an earlier method using τ as a parameter.

The summary of the rest of the paper is as follows. The CDE is introduced and the unique existence and regularity of its solution are considered in Section 2. A generalized EVP derived from the CDE is presented in Section 3, and the solution to the CDE is expressed in terms of an infinite series involving the corresponding eigenvectors and eigenvalues in Section 4. Numerical results based on the theory developed in the previous sections are presented in Section 5. Concluding remarks that explain the advantages of this method and some possible disadvantages along with scope for the future work are given in Section 6.

2. Correlation diffusion equation

Let $\Omega \subset \mathbb{R}^n$, $n = 2$ or 3 be a bounded domain with a $C^{1,1}$ boundary. The propagation of the field autocorrelation ϕ_τ in a turbid medium irradiated with a near-infrared light source f obeys the CDE [10]:

$$\begin{aligned} -\nabla\cdot(\kappa\nabla\phi_\tau) + (\mu + g_\tau b)\phi_\tau &= f \qquad \text{in } \Omega, \\ \phi_\tau + \nu\cdot\kappa\nabla\phi_\tau &= 0 \qquad \text{on } \partial\Omega, \end{aligned} \tag{1}$$

where $\nu \in C^{0,1}(\partial\Omega, \mathbb{R}^n)$ is the exterior unit normal of Ω, $\kappa \in C^{0,1}(\overline{\Omega}, \mathbb{R}^{n\times n})$ is the symmetric and Lipschitz continuous diffusion tensor, and $\mu \in L^\infty(\Omega)$ is the real-valued absorption coefficient. Furthermore, g_τ and $b \in L^\infty(\Omega)$ are application-specific real-valued coefficients that depend on the decorrelation time and the spatial variable, respectively; the map $\mathbb{R}_+ := [0,\infty) \ni \tau \mapsto g_\tau \in \mathbb{R}$ is assumed to be continuous throughout this work. In what follows, we occasionally interpret the field autocorrelation ϕ_τ as a function of two variables by writing $\phi_\tau(x) = \phi(x,\tau)$. For a fixed but arbitrary $\tau \in \mathbb{R}_+$ and $f \in L^2(\Omega)$, the variational formulation of (1) is to find $\phi_\tau \in H^1(\Omega)$ such that (cf., e.g., [12, §2.2.1])

$$B(\phi_\tau, v) := \int_\Omega (\kappa\nabla\phi_\tau\cdot\nabla\overline{v} + (\mu + g_\tau b)\phi_\tau\overline{v})\,\mathrm{d}x + \int_{\partial\Omega}\phi_\tau\overline{v}\,\mathrm{d}s = \int_\Omega f\overline{v}\,\mathrm{d}x =: b(v)$$

for all $v \in H^1(\Omega)$. Here and in the following, the L^2-based Sobolev spaces are defined over the complex field $\mathbb{C}$.

Remark 1

For scattering particles undergoing Brownian motion in DWS, we have $g_\tau = \tau$ and $b = 2\mu_s' k_0^2 D_B$, where μ_s' is the reduced scattering coefficient, $k_0 = 2\pi/\lambda_0$ is the modulus of the wave vector of the light source f, and D_B is the particle diffusion coefficient, describing a mechanical property of the object [5]. Similarly, in UMOT, it holds that $b = \mu_s' p$ and $g_\tau = \sin^2(\omega_a\tau/2)$, where p is the mean-squared amplitude of vibration of scattering particles under the influence of US with frequency ω_a [10]. For more information on the physical models of DWS and UMOT and their connections with (1), we refer to [5, 10, 11] and the references therein.

Throughout this text, we assume that there exist positive real constants $\kappa_0, c_0 > 0$ such that the estimates

$$\kappa \geq \kappa_0 I \quad \text{and} \quad \mu + g_\tau b \geq c_0 \tag{2}$$

hold for every $\tau \in \mathbb{R}_+$ and almost everywhere in Ω. Here, $I \in \mathbb{R}^{n\times n}$ denotes the identity matrix, and the first inequality is to be understood in the sense of positive definiteness. The following theorem and corollary are consequences of basic results on elliptic PDEs [12].

Theorem 2.1
Assume that $f \in L^2(\Omega)$. Then, the problem (1) has a unique (weak) solution $\phi_\tau \in H^2(\Omega)$ for all $\tau \in \mathbb{R}_+$. Furthermore, the solution map

$$(\tau, f) \mapsto \phi_\tau, \quad \mathbb{R}_+ \times L^2(\Omega) \to H^2(\Omega) \tag{3}$$

is continuous; in particular,

$$\|\phi_\tau\|_{H^2(\Omega)} \leq C_\tau \|f\|_{L^2(\Omega)}, \tag{4}$$

where $C_\tau > 0$ is independent of f and can be chosen to depend continuously on $\tau \in \mathbb{R}_+$.

Proof
The fact that (1) has a unique solution $\phi_\tau \in H^2(\Omega)$ for any $\tau \in \mathbb{R}_+$ follows directly from [12, Theorem 2.4.2.6](unique existence and regularity), the proof of which also readily demonstrates that (4) is valid for some $C_\tau > 0$.

Let us then prove that the map (3) is continuous. The existence of the solution ϕ_τ coupled with (4) shows that the differential operator

$$D_\tau : v \mapsto -\nabla \cdot (\kappa \nabla v) + (\mu + g_\tau b)v$$

is invertible as a linear map from

$$H^2_{\mathrm{R},0}(\Omega) := \left\{ v \in H^2(\Omega) \mid v + \nu \cdot \kappa \nabla v = 0 \text{ on } \partial\Omega \right\} \tag{5}$$

to $L^2(\Omega)$ for any $\tau \in \mathbb{R}_+$. Take note that $H^2_{\mathrm{R},0}(\Omega)$ is a well-defined closed subspace of $H^2(\Omega)$ due to the trace theorem [12, Theorem 1.5.1.2]; in particular, $H^2_{\mathrm{R},0}(\Omega)$ is itself a Hilbert space. The inverse $D_\tau^{-1} : L^2(\Omega) \to H^2_{\mathrm{R},0}(\Omega) \subset H^2(\Omega)$ realizes the solution map of (3), and thus, the assertion follows by showing that D_τ^{-1} depends continuously on $\tau \in \mathbb{R}_+$ in the operator topology of $\mathcal{L}(L^2(\Omega), H^2(\Omega))$.

Let $\{\tau_j\}_{j=1}^\infty \subset \mathbb{R}_+$ be a sequence that converges to arbitrary but fixed $\tau \in \mathbb{R}_+$ and consider the (compact) linear operator

$$T_j : v \mapsto (g_\tau - g_{\tau_j})bv, \quad H^2(\Omega) \to L^2(\Omega),$$

which vanishes in the operator topology as j tends to infinity because of the continuity of the map $\tau \mapsto g_\tau$. Without loss of generality, we may thus assume that

$$\|T_j\|_{\mathcal{L}(H^2(\Omega),L^2(\Omega))} \|D_\tau^{-1}\|_{\mathcal{L}(L^2(\Omega),H^2(\Omega))} \leq \frac{1}{2}, \qquad j = 1, 2, \ldots .$$

Because $D_{\tau_j} = D_\tau - T_j$, we have

$$D_\tau^{-1} - D_{\tau_j}^{-1} = D_\tau^{-1} \left(I - \left(I - T_j D_\tau^{-1} \right)^{-1} \right) = -D_\tau^{-1} \sum_{k=1}^{\infty} \left(T_j D_\tau^{-1} \right)^k$$

by virtue of the Neumann series representation for the inverse. In consequence,

$$\|D_\tau^{-1} - D_{\tau_j}^{-1}\| \leq \|D_\tau^{-1}\| \sum_{k=1}^{\infty} \|T_j\|^k \|D_\tau^{-1}\|^k = \frac{\|T_j\| \|D_\tau^{-1}\|^2}{1 - \|T_j\| \|D_\tau^{-1}\|} \leq 2\|T_j\| \|D_\tau^{-1}\|^2,$$

which converges to zero as j tends to infinity. As $\tau \in \mathbb{R}_+$ was arbitrary, this completes the proof. □

Corollary 2.2
Under the assumptions of Theorem 2.1, the unique solution of (1) satisfies

$$\|\phi_\tau\|_{H^1(\Omega)} \leq C \|f\|_{L^2(\Omega)},$$

where $C = (\min\{\kappa_0, c_0\})^{-1}$ is independent of both $f \in L^2(\Omega)$ and $\tau \in \mathbb{R}_+$.

Proof
Consider the variation formulation of (1) introduced earlier. Obviously, the antilinear functional $b : H^1(\Omega) \to \mathbb{C}$ is bounded, and the sesquilinear form $B : H^1(\Omega) \times H^1(\Omega) \to \mathbb{C}$ is bounded and coercive, that is,

$$|B(w, v)| \leq C \|w\|_{H^1(\Omega)} \|v\|_{H^1(\Omega)} \quad \text{and} \quad B(w, w) \geq \min\{\kappa_0, c_0\} \|w\|^2_{H^1(\Omega)}$$

for all $w, v \in H^1(\Omega)$. In consequence, the unique solvability of (1) in $H^1(\Omega)$ follows from the Lax–Milgram lemma [12, 2.2.1.1]; this H^1-solution naturally coincides with $\phi_\tau \in H^2(\Omega)$ of Theorem 2.1. In particular, it holds that

$$\min\{\kappa_0, c_0\} \|\phi_\tau\|^2_{H^1(\Omega)} \leq B(\phi_\tau, \phi_\tau) = \int_\Omega f \overline{\phi}_\tau \, \mathrm{d}x \leq \|f\|_{L^2(\Omega)} \|\phi_\tau\|_{L^2(\Omega)},$$

which proves the claim. □

3. A generalized eigenvalue problem

Let us make two more assumptions on the coefficients of (1), namely, that there exist constants $\mu_0, b_0 > 0$ such that

$$\mu \geq \mu_0 \quad \text{and} \quad b \geq b_0$$

almost everywhere in Ω. In particular, this allows us to define a weighted L^2-inner product

$$(v, w)_b := \int_\Omega b\, v\overline{w}\, \mathrm{d}x, \qquad v, w \in L^2(\Omega),$$

and argue that the induced norm $\|\cdot\|_b := (\cdot,\cdot)_b^{1/2}$ is equivalent to the standard L^2-norm:

$$b_0 \|v\|^2_{L^2(\Omega)} \leq \|v\|_b^2 \leq \|b\|_{L^\infty(\Omega)} \|v\|^2_{L^2(\Omega)}. \tag{6}$$

Notice that $L^2(\Omega)$ remains a Hilbert space if equipped with the inner product $(\cdot,\cdot)_b$ instead of the standard one.

Recall the definition of $H^2_{\mathrm{R},0}(\Omega)$ from (5) and let us study the linear partial differential operator

$$L : v \mapsto \frac{1}{b}\left(-\nabla\cdot(\kappa\nabla v) + \mu v\right), \quad H^2_{\mathrm{R},0}(\Omega) \to L^2(\Omega),$$

with respect to the new b-dependent inner product.

Lemma 3.1
The partial differential operator $L : H^2_{\mathrm{R},0}(\Omega) \to L^2(\Omega)$ is self-adjoint with respect to the weighted inner product $(\cdot,\cdot)_b$, that is,

$$(Lv, w)_b = (v, Lw)_b$$

for all $v, w \in H^2_{\mathrm{R},0}(\Omega)$.

Proof
The assertion follows from a simple application of the Green's formula [12, Theorem 1.5.3.1], minding the homogeneous Robin condition in the definition of $H^2_{\mathrm{R},0}(\Omega)$. □

This observation leads straightforwardly to the following theorem.

Theorem 3.2
The generalized EVP

$$\begin{aligned} -\nabla\cdot(\kappa\nabla\varphi) + \mu\varphi &= \lambda b\varphi \quad && \text{in } \Omega, \\ \varphi + \nu\cdot\kappa\nabla\varphi &= 0 && \text{on } \partial\Omega \end{aligned} \tag{7}$$

has a countable number of solution pairs $\{(\lambda_j, \varphi_j)\}_{j=1}^\infty \subset \mathbb{R}_+ \times H^2(\Omega)$ such that the eigenfunctions $\{\varphi_j\}_{j=1}^\infty$ form an $(\cdot,\cdot)_b$-orthonormal basis of $L^2(\Omega)$. Moreover, the corresponding eigenvalues (arranged in ascending order) satisfy

$$\lambda_1 \geq \operatorname*{ess\,inf}_{x\in\Omega} \frac{\mu(x)}{b(x)} \geq \frac{\mu_0}{\|b\|_{L^\infty(\Omega)}} \qquad \text{and} \qquad \lim_{j\to\infty} \lambda_j = \infty. \tag{8}$$

Proof
Let $g \in L^2(\Omega)$ be arbitrary and consider the boundary value problem

$$\begin{aligned} -\nabla\cdot(\kappa\nabla v) + \mu v &= bg \quad && \text{in } \Omega, \\ v + \nu\cdot\kappa\nabla v &= 0 && \text{on } \partial\Omega. \end{aligned} \tag{9}$$

Because of basic theory on elliptic boundary value problems [12, Theorem 2.4.2.6], (9) has a unique solution $v \in H^2(\Omega)$ satisfying

$$\|v\|_{H^2(\Omega)} \leq C\|bg\|_{L^2(\Omega)} \leq C\|b\|_{L^\infty(\Omega)}\|g\|_{L^2(\Omega)},$$

where $C > 0$ is independent of b and g. In particular, it follows that the operator $L : H^2_{\mathrm{R},0}(\Omega) \to L^2(\Omega)$ is invertible, with its inverse given by the bounded map

$$L^{-1} : g \mapsto v, \quad L^2(\Omega) \to H^2_{\mathrm{R},0}(\Omega) \subset H^2(\Omega),$$

where v is the solution of (9).

Because the embedding $H^2(\Omega) \hookrightarrow L^2(\Omega)$ is compact [12, Theorem 1.4.3.2], L^{-1} is compact as a mapping of $L^2(\Omega)$ into itself. Moreover, L^{-1} is self-adjoint with respect to $(\cdot,\cdot)_b$ because of Lemma 3.1. As L^{-1} is injective, that is, does not have zero as an eigenvalue, the assertion about the countability of the solution pairs of (7), the claimed properties of the corresponding eigenfunctions, and the second part of (8) follow from the spectral theory for compact and self-adjoint operators on Hilbert spaces [13, Chap. VIII, §2]. (Notice that (λ_j, φ_j) is a solution of (7) if and only if $(\lambda_j^{-1}, \varphi_j)$ is an eigenpair for L^{-1}.)

Finally, for any $\|\cdot\|_b$-normalized eigenpair $(\lambda_j, \varphi_j) \in \mathbb{R} \times H^2(\Omega)$ of (7) it holds that

$$\begin{aligned}\lambda_j = \lambda_j(\varphi_j, \varphi_j)_b &= \int_\Omega (-\nabla\cdot(\kappa\nabla\varphi_j) + \mu\varphi_j)\,\overline{\varphi}_j\,\mathrm{d}x \\ &= \int_\Omega \left(\kappa\nabla\varphi_j\cdot\nabla\overline{\varphi}_j + \mu|\varphi_j|^2\right)\mathrm{d}x + \int_{\partial\Omega}|\varphi_j|^2\mathrm{d}s \\ &\geq \int_\Omega \frac{\mu}{b} b|\varphi_j|^2\mathrm{d}x \geq \operatorname*{ess\,inf}_{x\in\Omega}\frac{\mu(x)}{b(x)},\end{aligned}$$

where we used the Green's formula and the boundary condition of (7). This proves the first part of (8) and completes the proof. □

Remark 2
Theorem 3.2 allows to write a decomposition of any $v \in L^2(\Omega)$ in the basis $\{\varphi_j\}_{j=1}^\infty$, that is,

$$v = \sum_{j=1}^\infty (v, \varphi_j)_b\,\varphi_j,$$

where the convergence is in the norm $\|\cdot\|_b$ and thus also in the standard topology of $L^2(\Omega)$ because of (6).

4. Generalized eigenvalue decomposition of $\phi_\tau(x)$

In this section, we demonstrate how one can separate the functional dependence of ϕ_τ on the decorrelation time $\tau \in \mathbb{R}_+$ and on the spatial variable.

Theorem 4.1
The solution of the CDE (1) can be represented as the series

$$\phi_\tau = \sum_{j=1}^\infty \frac{(f,\varphi_j)_{L^2(\Omega)}}{\lambda_j + g_\tau}\,\varphi_j, \tag{10}$$

which converges in $H^1(\Omega)$ uniformly over $\tau \in \mathbb{R}_+$ and in $H^2(\Omega)$ uniformly over $\tau \in U$ for any bounded $U \subset \mathbb{R}_+$. Here, $\{(\lambda_j, \varphi_j)\}_{j=1}^\infty \subset \mathbb{R}_+ \times H^2(\Omega)$ are the eigenpairs from Theorem 3.2.

Proof
To begin with, note that all terms in the sum (10) are well defined because for any $\tau \geq 0$ and $j \in \mathbb{N}$,

$$\lambda_j + g_\tau \geq \operatorname*{ess\,inf}_{x\in\Omega}\frac{\mu(x)}{b(x)} + g_\tau \geq \frac{c_0}{\|b\|_{L^\infty(\Omega)}} > 0$$

by virtue of Theorem 3.2 and the assumption (2).

Fix $\tau \in \mathbb{R}_+$ and consider the partial sum up to $m \in \mathbb{N}$,

$$\phi_\tau^{(m)} := \sum_{j=1}^m \frac{(f,\varphi_j)_{L^2(\Omega)}}{\lambda_j + g_\tau}\,\varphi_j. \tag{11}$$

By changing the order of differentiation and the finite summation, one immediately obtains that

$$\begin{aligned}-\nabla\cdot\left(\kappa\nabla\phi_\tau^{(m)}\right) + (\mu + g_\tau b)\phi_\tau^{(m)} &= \sum_{j=1}^m \frac{(f,\varphi_j)_{L^2(\Omega)}}{\lambda_j + g_\tau}\lambda_j b\varphi_j + \sum_{j=1}^m \frac{(f,\varphi_j)_{L^2(\Omega)}}{\lambda_j + g_\tau} g_\tau b\varphi_j \\ &= b\sum_{j=1}^m (f,\varphi_j)_{L^2(\Omega)}\,\varphi_j =: f^{(m)}.\end{aligned}$$

In other words, $\phi_\tau^{(m)}$ satisfies the boundary value problem

$$\begin{aligned}-\nabla\cdot(\kappa\nabla\phi_\tau^{(m)}) + (\mu + g_\tau b)\phi_\tau^{(m)} &= f^{(m)} \quad &&\text{in } \Omega, \\ \phi_\tau^{(m)} + \nu\cdot\kappa\nabla\phi_\tau^{(m)} &= 0 &&\text{on } \partial\Omega.\end{aligned}$$

The claim thus follows from Theorem 2.1 and Corollary 2.2 if $f^{(m)}$ converges to f in $L^2(\Omega)$. The latter can be demonstrated with ease:

$$\|f - f^{(m)}\|_{L^2(\Omega)} \leq \|b\|_{L^\infty(\Omega)} \left\| \frac{f}{b} - \sum_{j=1}^{m} \left(\frac{f}{b}, \varphi_j \right)_b \varphi_j \right\|_{L^2(\Omega)} \to 0$$

as $m \to \infty$, due to Theorem 3.2. □

4.1. *Measurement maps*

The measurement map corresponding to the CDE is defined as the τ-parameterized operator sending the source term in (1) to the Dirichlet boundary value of the corresponding solution, that is,

$$F_\tau : f \mapsto \phi_\tau|_{\partial\Omega}, \quad L^2(\Omega) \to H^{3/2}(\partial\Omega) \subset H^{1/2}(\partial\Omega) \subset L^2(\partial\Omega), \qquad \tau \in \mathbb{R}_+.$$

It is well defined and bounded in accordance with Theorem 2.1, Corollary 2.2, and the trace theorem [12, Theorem 1.5.1.2]. The mapping F_τ is essential when solving parameter estimation problems corresponding to the CDE, as it characterizes the relationship between the excitation and the boundary measurement. Allowing an oversimplification, the nonlinear dependence of F_τ on the coefficients of the CDE is what is being inverted when solving the inverse problem of UMOT or that of DWS. If the chosen inversion technique is some regularized output least squares method, the outputs of certain operators closely related to F_τ and its adjoint typically need to be evaluated repetitively for varying inputs and coefficients of the CDE (see, e.g., [11]). Theorem 4.1 provides means to represent F_τ efficiently with the help of certain generalized eigenpairs of a related differential operator that is independent τ, but analogous representations for the adjoint F_τ^* still merit some further analysis.

The L^2-adjoint of F_τ is the unique τ-parameterized map

$$F_\tau^* : L^2(\partial\Omega) \to L^2(\Omega), \qquad \tau \in \mathbb{R}_+$$

that satisfies

$$(F_\tau f, h)_{L^2(\partial\Omega)} = \left(f, F_\tau^* h\right)_{L^2(\Omega)} \qquad \text{for all } f \in L^2(\Omega),\ h \in L^2(\partial\Omega)$$

and any $\tau \in \mathbb{R}_+$. A straightforward application of the Green's formula shows that F_τ^* can be characterized by

$$F_\tau^* : h \mapsto \psi_\tau,$$

where $\psi_\tau \in H^1(\Omega) \subset L^2(\Omega)$, $\tau \in \mathbb{R}_+$, is the unique solution of

$$\begin{aligned} -\nabla \cdot (\kappa \nabla \psi_\tau) + (\mu + g_\tau b)\psi_\tau &= 0 \quad \text{in } \Omega, \\ \psi_\tau + \nu \cdot \kappa \nabla \psi_\tau &= h \quad \text{on } \partial\Omega \end{aligned} \tag{12}$$

for $h \in L^2(\partial\Omega)$ [12]. By slightly modifying the arguments in the proof of Corollary 2.2, it follows that

$$\|\psi_\tau\|_{H^1(\Omega)} \leq C \|h\|_{L^2(\partial\Omega)},$$

where $C > 0$ is independent of $\tau \in \mathbb{R}_+$. Like ϕ_τ, also ψ_τ allows a spectral decomposition.

Corollary 4.2
The solution of (12) can be represented as the series

$$\psi_\tau = \sum_{j=1}^{\infty} \frac{(h, \varphi_j)_{L^2(\partial\Omega)}}{\lambda_j + g_\tau} \varphi_j, \tag{13}$$

which converges in $L^2(\Omega)$ for any $\tau \in \mathbb{R}_+$. Here, $\{(\lambda_j, \varphi_j)\}_{j=1}^{\infty} \subset \mathbb{R}_+ \times H^2(\Omega)$ are the eigenpairs from Theorem 3.2.

Proof
By (7) and (12), we have

$$\begin{aligned} (h, \varphi_j)_{L^2(\partial\Omega)} &= \int_{\partial\Omega} \left(\nu \cdot \kappa \nabla \psi_\tau \, \overline{\varphi}_j - \psi_\tau \, \nu \cdot \kappa \nabla \overline{\varphi}_j \right) \mathrm{d}s \\ &= \int_\Omega \left(\nabla \cdot (\kappa \nabla \psi_\tau) \, \overline{\varphi}_j - \psi_\tau \nabla \cdot \left(\kappa \nabla \overline{\varphi}_j \right) \right) \mathrm{d}x \\ &= \int_\Omega \left((\mu + g_\tau b) \psi_\tau \overline{\varphi}_j - (\mu - \lambda_j b) \psi_\tau \overline{\varphi}_j \right) \mathrm{d}x \\ &= (\lambda_j + g_\tau)(\psi_\tau, \varphi_j)_b, \end{aligned}$$

where we also used a weak version of the Green's formula (cf., e.g., [12, Remark 1.5.3.5]). In consequence, it holds that

$$\sum_{j=1}^{m} \frac{(h,\varphi_j)_{L^2(\partial\Omega)}}{\lambda_j + g_\tau}\,\varphi_j = \sum_{j=1}^{m} (\psi_\tau,\varphi_j)_b \varphi_j \to \psi_\tau \qquad \text{as } m \to \infty,$$

where the convergence is in $L^2(\Omega)$ (cf. Theorem 3.2). □

Take note that—apart from the trivial case $h \equiv 0$—the series (13) does *not* converge in $H^1(\Omega)$ because it cannot satisfy the boundary condition of (12). Although convergence in $L^2(\Omega)$ is often enough from the practical point of view, this slight imperfection can also be fixed with the help of the unique solution $\psi \in H^1(\Omega)$ of the τ-independent inhomogeneous Robin problem

$$\begin{aligned} -\nabla\cdot(\kappa\nabla\psi) + \mu\psi &= 0 \quad && \text{in } \Omega, \\ \psi + \nu\cdot\kappa\nabla\psi &= h && \text{on } \partial\Omega. \end{aligned}$$

The following corollary presents a computationally more expensive decomposition with better convergence properties.

Corollary 4.3
The solution of (12) can be represented in the form

$$\psi_\tau = \psi - g_\tau \sum_{j=1}^{\infty} \frac{(\psi,\varphi_j)_b}{\lambda_j + g_\tau}\,\varphi_j,$$

where the sum converges in $H^2(\Omega)$ uniformly over $\tau \in U$ for any bounded $U \subset \mathbb{R}_+$. Here, $\{(\lambda_j,\varphi_j)\}_{j=1}^{\infty} \subset \mathbb{R}_+ \times H^2(\Omega)$ are the eigenpairs from Theorem 3.2.

Proof
The difference $\tilde{\psi}_\tau := \psi_\tau - \psi$ obviously satisfies

$$\begin{aligned} -\nabla\cdot\left(\kappa\nabla\tilde{\psi}_\tau\right) + (\mu + g_\tau b)\tilde{\psi}_\tau &= -g_\tau b\psi \quad && \text{in } \Omega, \\ \tilde{\psi}_\tau + \nu\cdot\kappa\nabla\tilde{\psi}_\tau &= 0 && \text{on } \partial\Omega. \end{aligned}$$

In consequence, it follows from Theorem 4.1 (and the assumed continuity of g_τ) that

$$\tilde{\psi}_\tau = \sum_{j=1}^{\infty} \frac{(-g_\tau b\psi,\varphi_j)_{L^2(\Omega)}}{\lambda_j + g_\tau}\,\varphi_j = -g_\tau \sum_{j=1}^{\infty} \frac{(\psi,\varphi_j)_b}{\lambda_j + g_\tau}\,\varphi_j,$$

with the claimed type of convergence. This completes the proof. □

5. Numerical results

In our numerical studies, $\Omega \subset \mathbb{R}^2$ is an origin-centered disk of radius 4 cm, and we have chosen the homogeneous isotropic values $\mu = 0.1\,\text{cm}^{-1}$, $\kappa = 0.0412\,\text{cm}$, and $\mu_s' = 8\,\text{cm}^{-1}$ for the absorption, diffusion, and reduced scattering coefficients, respectively. The other parameters appearing in (1) and (7) are application-specific and defined separately in Sections 5.1 and 5.2 (cf. Remark 1). The numerical solution of (1) and (7) is based on a *finite element method* (FEM) with piecewise linear basis functions. Unless stated otherwise, the FEM discretization of Ω consists of 1933 nodes and 3726 triangular elements. The source f of (1) is chosen to have nonzero value only at a single node positioned at (3.875 cm, 0 cm), which is one scattering length inside the boundary, and to integrate to 1 over the domain Ω. This is a typical way of modeling the near-infrared light illumination in DOT (see, e.g., [3]).

For given parameter values, the CDE (1) is solved approximately for ϕ_τ at a number of correlation times $\tau \in \mathbb{R}_+$ using two approaches:

I The discretized linear system originating from (1) is solved for one τ at a time by the `mldivide` operation of MATLAB.
II The FEM-discretized version of the generalized EVP (7) is solved by the `eigs` command of MATLAB, and subsequently, ϕ_τ is evaluated at different values of τ via the discretized counterpart of (10). (In particular, there are only as many eigenpairs as there are degrees of freedom in the FEM discretization, and thus, the summation in the discretized version of (10) is finite.)

Remark 3
We have simply used the MATLAB commands `mldivide` and `eigs` in the definitions of our solution methods because we do not want to consider the implementation and efficiency of standard algorithms of numerical linear algebra. Of these commands, `mldivide` solves a matrix equation exactly (up to rounding errors) using a noniterative algorithm that is chosen according to the properties of the system matrix, whereas `eigs` is based on the Arnoldi iteration (see, e.g., [14]) and computes a chosen number of (generalized) eigenvalues and eigenvectors up to some user-specified tolerance. In particular, the fewer eigenpairs are required, the faster the performance of `eigs` is. We have used the default parameter values for `eigs` in our implementation of method II.

In what follows, we consider the forward problems of DWS and UMOT separately.

5.1. Numerical solution of the diffusing wave spectroscopy forward problem

We first consider the case of particles undergoing Brownian motion in DWS, that is, choose $g_\tau = \tau$ and $b = 2\mu_s' k_0^2 D_B$ in (1). The optical and mechanical properties used in the numerical simulations for the DWS forward problem are chosen as $k_0 = 2\pi/\lambda_0 = 9.9683 \times 10^4$ cm ($\lambda_0 = 630 \times 10^{-7}\text{cm}^{-1}$) and

$$D_B(x) = \begin{cases} 5 \times 10^{-9}\ \text{cm}^2/\text{s}, & |x| \le 0.8\ \text{cm}, \\ 10^{-9}\ \text{cm}^2/\text{s}, & \text{otherwise}. \end{cases}$$

Take note that D_B is given an inhomogeneous distribution to make b of (1) nonconstant, and subsequently (7) a generalized EVP instead of a standard one. For DWS, we consider decorrelation times between 10^{-9} and 10^{-3} s.

Figure 1(a) shows a grey level plot of the approximation of ϕ_τ given by method I as a function of the spatial variable at the decorrelation time $\tau = 10^{-9}$ s, whereas Figure 1(b) visualizes the difference between the solutions given by I and II. According to Figure 1(b), there is a *Gibbs-like* mismatch between the two approximate solutions when confined to the boundary of Ω. To elaborate on this phenomenon, we have plotted the approximates for $\phi_\tau|_{\partial\Omega}$, at $\tau = 10^{-9}$ s and $\tau = 4.9 \times 10^{-4}$ s, with respect to the polar angle in Figure 2. We have only considered the values of $\phi_\tau|_{\partial\Omega}$ between 26 and 334 degrees (measuring from the source position), due to the small size of the discrepancy between the two solutions compared with the absolute value of $\phi_\tau|_{\partial\Omega}$ close to the source position.

According to our numerical experiments, the qualitative properties of the solutions provided by I and II are similar to what is visualized in Figures 1 and 2 also for other values of τ between 10^{-9} and 10^{-3} s. The approach II, based on the generalized eigenvalue expansion, seems to promote slightly unreliable oscillating approximations for the field autocorrelation ϕ_τ close to the object boundary, but this discrepancy is small compared with the overall range of values for ϕ_τ.

The computational times needed for solving the DWS forward problem for four FEM discretizations of Ω and different number of values for τ are shown in Table I. As the number of decorrelation time samples increases, the computational time for I becomes considerably larger than that required by II. On the other hand, as discretization gets finer, the higher computational efficiency of II compared with I occurs only for large number of τ samples. There is a natural explanation for the latter phenomenon: The computational time

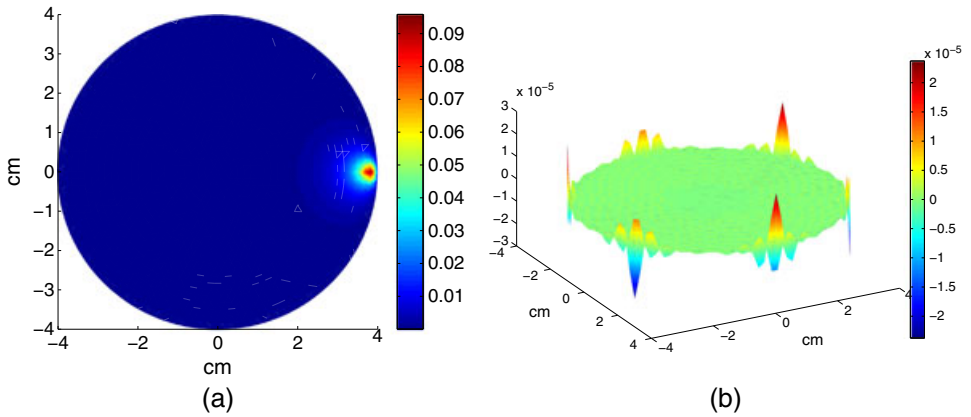

Figure 1. Forward solution of diffusing wave spectroscopy. (a) Approximation of ϕ_τ at $\tau = 10^{-9}$ s by method I. (b) The difference between the approximations provided by methods I and II at $\tau = 10^{-9}$ s. (Notice the different color scales of the subfigures.)

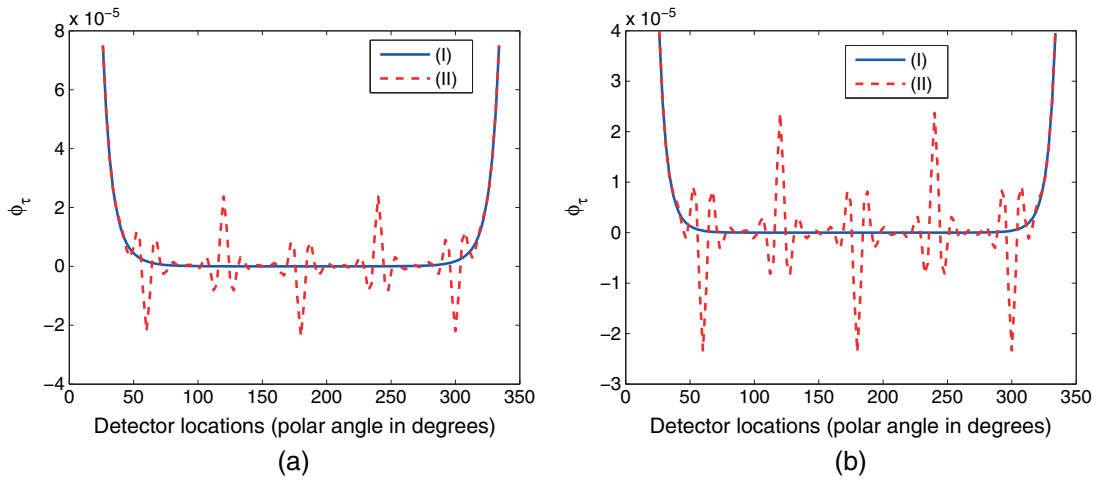

Figure 2. Forward solution of diffusing wave spectroscopy by methods I and II restricted to $\partial\Omega$ for (a) $\tau = 10^{-9}$ s and (b) $\tau = 4.9 \times 10^{-4}$ s.

Table I. Computational times in seconds required by I and II for different number of discretization points for τ in the case of diffusing wave spectroscopy. From left to right: a mesh with 1243 nodes and 2376 elements, a mesh with 1933 nodes and 3726 elements, a mesh with 2773 nodes and 5376 elements, and a mesh with 4663 nodes and 9102 elements.

#τ	I	II	I	II	I	II	I	II
10	0.812	8.173	1.375	27.136	2.625	125.961	5.803	627.517
100	7.685	9.184	13.393	31.444	25.134	134.225	48.391	668.713
1000	73.875	23.250	132.936	62.452	247.130	193.701	572.948	813.903
5000	370.353	83.905	736.500	203.031	1463.048	481.582	2819.471	1576.567

for obtaining the eigenpairs needed in the discretized version of (10) grows faster as a function of the dimension of the linear system than the time consumption of solving a (sparse) matrix equation of the same size. Thus, the number of correlation times needed for demonstrating the computational advantage of II over I is monotonically increasing as a function of the size of the considered discretized systems. Although the computation times listed in Table 1 certainly depend on the hardware, the relative performance of the two methods should be approximately independent of the hardware specifications. Here, we used a PC with Intel-core i5 having a processor speed of 2.5 GHz.

For method II, the computation of all the eigenpairs corresponding to the FEM-discretized version of (7) is definitely an exaggeration, as the discretized version of the series representation (10) gives a reasonable approximation for the autocorrelation field ϕ_τ already for considerably lower number of eigenmodes. (Recall that there are as many discrete eigenpairs as there are nodes in the FEM mesh, that is, 1933 in our case.) To verify this claim, we have plotted in Figure 3 the relative $L^2(\Omega)$-error between the approximate solutions of (1) obtained by methods I and II, respectively, as a function of the number of the (smallest) eigenvalues and eigenvectors used in the discretized version of (10) for II. Two different decorrelation times $\tau = 10^{-9}$ s and $\tau = 10^{-3}$ s are considered. If the solution provided by I is considered as the ground truth, then one-third of the eigenpairs for II seems to be enough for a relative $L^2(\Omega)$-error of less than 1% for all values of τ between 10^{-9} and 10^{-3} s. Moreover, the convergence speed of (10) definitely depends on the regularity of the source f, which is rather spiky in our computations. In consequence, if some other application deals with smoother sources, the number of required eigenpairs for (10) is probably reduced, making method II computationally more attractive.

5.2. *Numerical solution of the ultrasound-modulated optical tomography forward problem*

In the case of UMOT, we have $g_\tau = \sin^2(\pi f_a \tau)$ and $b = \mu_s' p$ in terms of (1). Here, $f_a = \omega_a/(2\pi) = 10^6$ MHz is the applied US frequency and p is defined piecewise via

$$p(x) = \begin{cases} 10^{-7}\ \text{cm}^2, & x \in D, \\ 10^{-9}\ \text{cm}^2, & \text{otherwise}, \end{cases} \tag{14}$$

where D is the disk of radius 1.5 cm centered at (1.5 cm, 0 cm). For UMOT, we consider decorrelation times between 0 and 2×10^{-6} s.

Figures 3–6 are organized in the same way as Figures 1–3 of the previous section. To be a bit more precise, Figure 4(a) illustrates the solution of the UMOT forward problem obtained by the conventional method I at $\tau = 8 \times 10^{-7}$ s, and Figure 4(b) shows the corresponding discrepancy between the solutions provided by I and II. The boundary values of the approximations of ϕ_τ provided by techniques I and II at $\tau = 0$ s and $\tau = 2 \times 10^{-6}$ s are visualized in Figure 5. Finally, Figure 6 demonstrates the convergence of the solution obtained

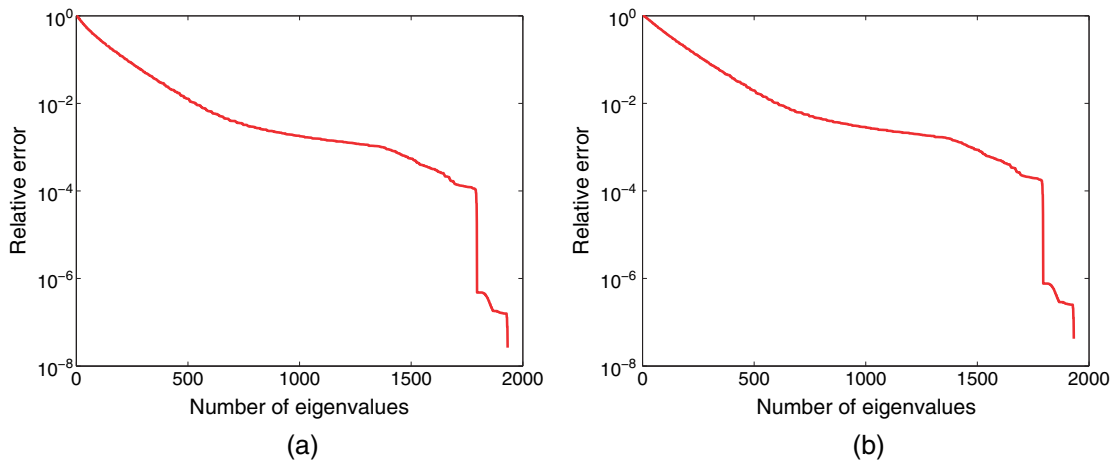

Figure 3. Diffusing wave spectroscopy: relative error between the solutions by I and II as a function of the number of eigenpairs used in (10) for II. (a) $\tau = 10^{-9}$ s and (b) $\tau = 10^{-3}$ s.

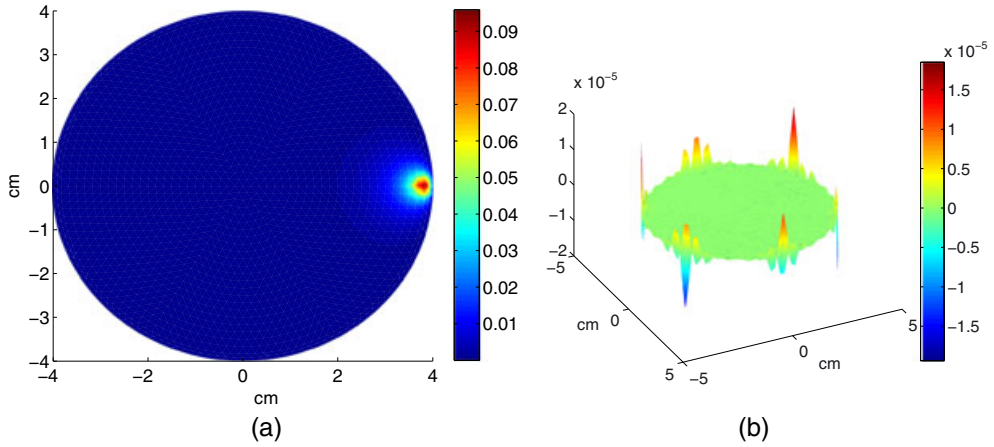

Figure 4. Forward solution of ultrasound-modulated optical tomography. (a) Approximation of ϕ_τ at $\tau = 8 \times 10^{-7}$ s by method I. (b) The difference between the approximations provided by methods I and II at $\tau = 8 \times 10^{-7}$ s. (Notice the different color scales of the subfigures.)

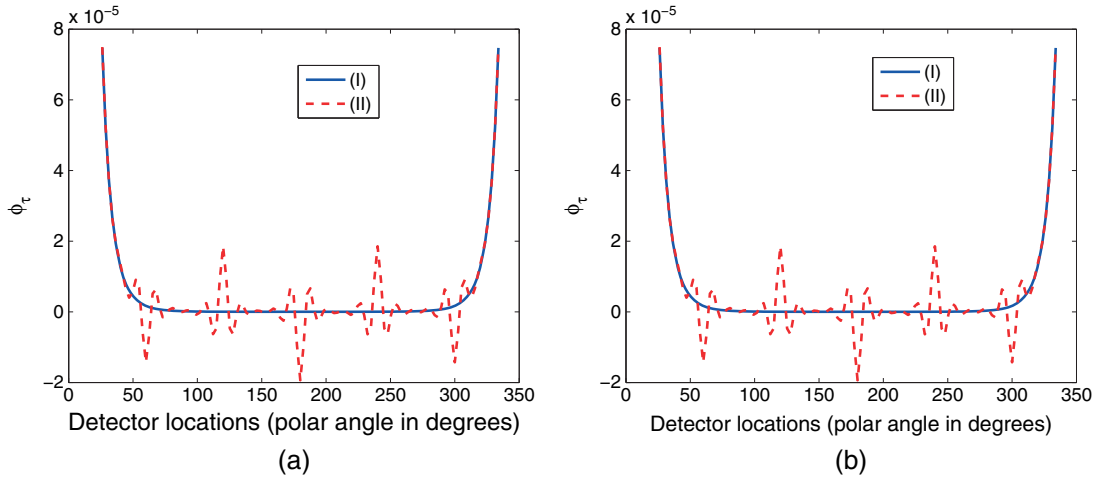

Figure 5. Forward solution of UMOT by the methods I and II restricted to $\partial\Omega$ for (a) $\tau = 0$ s and (b) $\tau = 2 \times 10^{-6}$s.

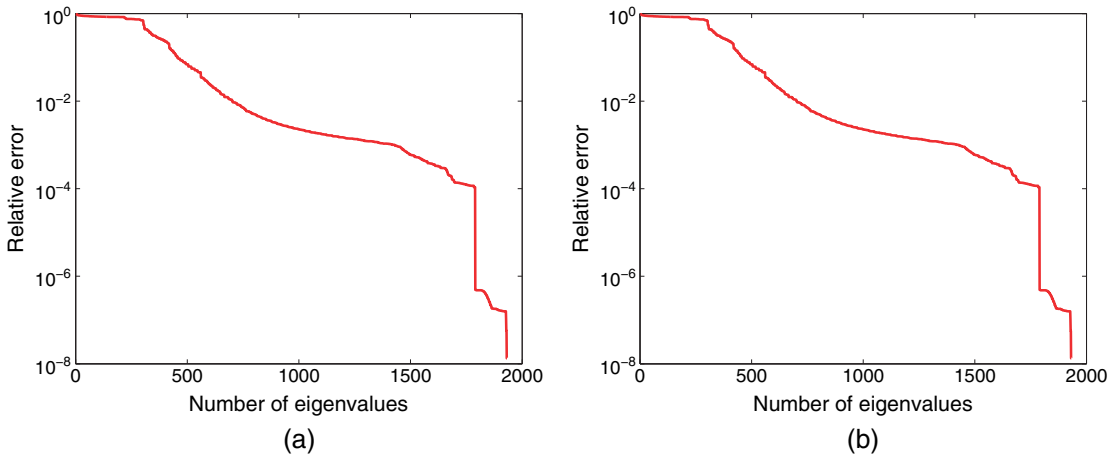

Figure 6. UMOT: Relative error between the solutions by I and II as a function of the number of eigenvalues used in (10) for II. (a) $\tau = 0$ s and (b) $\tau = 2 \times 10^{-6}$s.

by II toward that from I in the relative $L^2(\Omega)$-norm as the number of eigenpairs used in the discrete version of (10) increases. Apart from the nonsmooth behavior of the convergence plots in Figure 6 for small number of eigenvalues—caused possibly by the small value of b in the background (cf. (14))—the conclusions about the performance of the novel method II in comparison with the standard method I are the same as in the case of DWS.

Table II. Computational times in seconds required by I and II for different number of discretization points for τ in the case of ultrasound-modulated optical tomography. From left to right: a mesh with 1243 nodes and 2376 elements, a mesh with 1933 nodes and 3726 elements, a mesh with 2773 nodes and 5376 elements, and a mesh with 4663 nodes and 9102 elements.

$\#\tau$	I	II	I	II	I	II	I	II
10	0.874	9.181	1.390	29.793	2.976	152.638	6.005	615.387
100	7.939	9.344	12.754	31.384	26.077	174.697	51.763	633.124
1000	76.026	17.908	130.079	63.579	270.769	198.288	490.273	789.433
5000	373.448	56.033	730.125	206.657	1501.571	498.372	3115.037	1634.104

Table II lists the computational times required for solving the UMOT forward problem with four FEM discretizations and for different number of decorrelation times τ. Here, all available discrete eigenpairs are used for II. The conclusions are the same as for the DWS forward problem in Section 5.1: For high number of evaluations in the decorrelation time τ, the new method II is superior, but if the solution is needed only at a low number of decorrelation times, then the standard method I is recommendable.

6. Conclusion

We have presented a weighted eigenvalue-based approach to solve an elliptic PDE in which time appears only as a parameter without a time derivative of the dependent variable in the PDE. This approach is illustrated to be computationally efficient in comparison with the usual method wherein the PDE is solved repeatedly with time as a parameter to arrive at the time variation in the forward solution.

Using the elliptic PDE theory, in an appropriate Hilbert space setting, we have proven the uniqueness of the solution arrived at as an expansion in terms of eigenfunctions. For this, we first show that the solution operator for the spectral problem at hand is both compact and self-adjoint in a suitable sense. Then, drawing from the spectral theory of compact self-adjoint operators, we go on to show that the eigenvectors in question provide a complete orthonormal basis for the underlying Hilbert space with respect to a weighted inner product. In consequence, the solution to the PDE is expressed uniquely in terms of the eigenpairs obtained by solving the EVP.

Compared with the conventional numerical method involving separate solution of, say, the CDE at each decorrelation time, we show that our new technique offers a reduction in the overall computational burden when the solution is needed at many time samples. As an example, for a two-dimensional FEM discretization of the CDE by 2773 nodes and 5376 elements, this effect is observed if the solution is needed at more than 1000 decorrelation times. On the negative side, it is to be expected that the number of correlation times required for demonstrating the computational advantage of the proposed method is monotonically increasing as a function of the size of the considered discretized systems. The observed computational advantage should show forth prominently when dealing with a fully three-dimensional problem, as the inversion of the FEM system matrix is relatively more expensive in three dimensions than in two dimensions because of the more complicated structure of the FEM mesh, making repetitive solution of the parameter-dependent PDE even more expensive. The numerical accuracy of the novel solution method is comparable with the conventional one, except at the boundary where we notice an oscillation similar to the Gibb's phenomenon common to solutions using the Fourier basis.

The application where the computational advantage of the new method shows up prominently is the imaging problem where the CDE is the forward model that needs to be solved repeatedly in the inversion. We have left tackling such tomography problems using the new eigenvalue approach for a future publication.

Acknowledgements

The work of N. Hyvönen and H. M. Varma was supported by the Academy of Finland (the Centre of Excellence in Inverse Problems Research and project 135979). A. K. Nandakumaran and R. M. Vasu were partially supported by Council of Scientific and Industrial Research under the project no: 25(0194)/11/EMR-II dated 02/02/2011.

References

1. Wang L, Jacques SL, Zhao X. Continuous-wave ultrasonic modulation of scattered laser light to image objects in turbid media. *Optics Letters* 1995; **20**:629–631.
2. Kempe M, Larionov M, Zaslavsky D, Genack AZ. Acousto-optic tomography with multiply scattered light. *Journal of the Optical Society of America A* 1997; **14**:1151–1158.
3. Arridge SR. Optical tomography in medical imaging. *Inverse Problems* 1999; **15**:R41–R93.
4. Wang LV. Mechanisms of ultrasonic modulation of multiply scattered coherent light: an analytic model. *Physical Review Letters* 2001; **87**:043903.
5. Pine DJ, Weitz DA, Chaikin PM, Herbolzheimer E. Diffusing wave spectroscopy. *Physical Review Letters* 1988; **60**:1134–1137.
6. Maret G, Wolf PE. Multiple light scattering from disordered media. The effect of Brownian motion of scatterers. *Zeitschrift für Physik B: Condensed Matter* 1987; **65**:409–413.
7. Chandran RS, Roy D, Kanhirodan R, Vasu RM, Devi CU. Ultrasound modulated optical tomography: Young's modulus of the insonified region from measurement of natural frequency of vibration. *Optics Express* 2011; **19**:22837–22850.
8. Leutz W, Maret G. Ultrasonic modulation of multiply scattered light. *Physica B* 1995; **204**:14–19.

9. Yao G, Wang LV. Theoretical and experimental studies of ultrasound-modulated optical tomography in biological tissue. *Applied Optics* 2000; **39**:659–664.
10. Sakadžić S, Wang LV. Correlation transfer and diffusion of ultrasound-modulated multiply scattered light. *Physical Review Letters* 2006; **96**:163902.
11. Varma HM, Mohanan KP, Hyvönen N, Nandakumaran AK, Vasu RM. Ultrasound-modulated optical tomography: recovery of amplitude of vibration in the insonified region from boundary measurement of light correlation. *Journal of the Optical Society of America A* 2011; **28**:2322–2331.
12. Grisvard P. *Elliptic Problems in Nonsmooth Domains*. Pitman: Boston, 1985.
13. Dautray R, Lions J-L. *Mathematical Analysis and Numerical Methods for Science and Technology*, Vol. 3. Springer-Verlag: Berlin, 1990.
14. Lehoucq RB, Sorensen DC. Deflation techniques for an implicitly restarted Arnoldi iteration. *SIAM Journal on Matrix Analysis and Applications* 1996; **17**:789–821.